Effect of viscous forces on the performance of a surging wave energy converter

Majid Bhinder, Aurélien Babarit, Lionel Gentaz, Pierre Ferrant

Effect of Viscous Forces on the Performance of a Surging Wave Energy Converter

Majid A. Bhinder, Aurélien Babarit, Lionel Gentaz, Pierre Ferrant
LUNAM Université
Ecole Centrale de Nantes
LHEEA – UMR CNRS 6598
Nantes, France.

ABSTRACT

A generic Oscillating Surge Wave Energy Converter (OSWC) has been tested numerically against the impact of the viscous forces. The study makes use of both the linear potential theory as well as the computational fluid dynamics (CFD). A state-of-the-art time domain *wave-to-wire* numerical model of the wave energy converter (WEC) is developed. Viscous damping is then included using an additional *velocity squared* term from the Morison equation. A range of possible values for the drag coefficient (following various literary resources) were tested so that to establish the scale of the viscous impact regarding the annual power production (APP) of the WEC. Wave resource considered in these numerical tests cover regular and irregular incident waves. Analysis of the APP demonstrates the importance/sensitivity of having an accurate prediction of the drag coefficient. Moreover CFD has been shown to be a valid tool for evaluation of the unknown drag coefficient. For this the CFD model has been validated by comparing its findings with the previously published experimental (and also numerical) results of a 3D square cylinder. This CFD model is then employed to 3D cases of the surging device in order to refine the estimates of the viscous drag coefficient.

KEY WORDS:
Wave energy converter; WEC; numerical modelling; CFD; viscous damping; drag; Flow3d.

INTRODUCTION

Floating wave energy devices are usually designed to exhibit oscillatory motion in response to the surrounding waves. Interaction of waves and the device oscillations give rise to vortex shedding and the impact of the viscous forces may become important. In terms of the APP (annual power production – measure of the efficiency) of the WECs the role of the resulting viscous drag is to date quite vague. It is of crucial importance that the inter-relation between the viscous drag and the power efficiency of the device is known to the design engineer thus ensuring that the optimized power output is also cost effective.
This paper presents a preliminary attempt towards the assessment of the viscous drag in relation to the efficiency of a particular generic WEC designed to oscillate in surge mode only (Fig.1).

When using numerical modelling of WECs in order to determine power production, the BEM (boundary element method) is used, but despite being based on state-of-the-art tools, viscous loss tends to be disregarded. On the other hand CFD models claim to solve the flow field that takes care of the viscous phenomenon. This study benefits from both approaches – the BEM and the CFD – in order to achieve a more robust model for the numerical assessment of a WEC.

(Folley et al, 2005; Hals et al, 2007) has previously included viscous drag into the mathematical models of WECs but the drag coefficients were taken from existing literature.

However in this work we investigate the derivation of these coefficients using CFD and the power output of a floating WEC; with and without viscous drag. The methodology, mathematical model, followed by the setup of the simulations are discussed next.

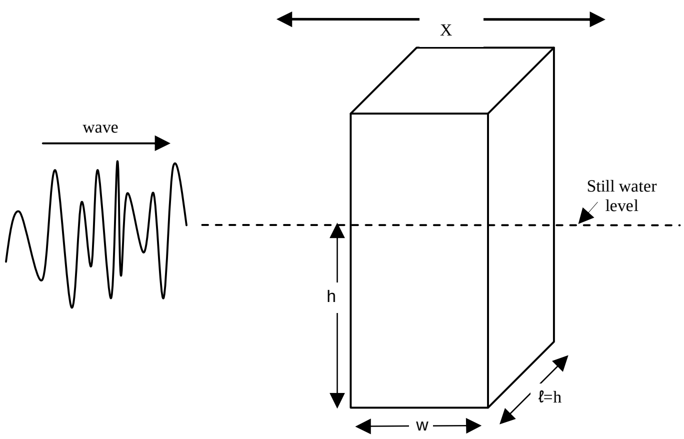

Fig.1 Schematic of the WEC. Where h= ℓ=10m,and w=7.85m

METHODOLOGY

Case study: a surging WEC

A 3d surging WEC with dimensions; height: 10m, length: 10m, width: 7.85m as described in (Babarit, 2010) was considered. The device is designed to oscillate in horizontal direction only. The schematic of the

WEC is shown in Fig.1.

Equation of motion

In time domain, within the frame of linear potential theory, the equation of motion can be written as

$$(M+\mu_\infty)\ddot{X}(t)=\begin{cases}F_{ex}(t)-\int_0^t K(t-\tau)d\tau \\ -B_{pto}\dot{X}(t)-K_{PTO}X(t)+F_{viscous}(t)\end{cases} \tag{1}$$

Here:

- $X(t)$: the displacement of the body
- $\dot{X}(t)$: velocity
- $\ddot{X}(t)$: acceleration
- $F_{ex}(t)$ is the excitation force of the incident waves. In irregular waves, for a given sea spectrum *S(f)*, a typical representation of the excitation force**,** is represented as $F_{ex}(t)=\Im\left(\sum_j A_j\tilde{F}_{ex}(f_j)e^{-i(2\pi f_j t+\varphi_j)}\right)$ in which the amplitudes A_j are given as $A_j=\sqrt{2S(f_j)\Delta f}$ **;** the phases φ_j are set randomly and $\tilde{F}_{ex}(f_j)$ are the complex excitation force coefficients which were calculated in the frequency domain.
- $-\mu_\infty\ddot{X}(t)-\int_0^t K(t-\tau)\dot{X}(\tau)d\tau$ is the radiation force. μ_∞ is the added mass coefficient and K is the retardation coefficient. These time domain coefficients were obtained from frequency domain coefficients using Ogilvie's formula. The numerical code Aquaplus was used to obtain the frequency domain coefficients.
- B_{pto} and K_{PTO} are the Power Take Off (PTO) damping and stiffness coefficients respectively.
- M is the mass of the body
- $F_{viscous}(t)$ is an additional force which exists only when viscous damping has been taken into account. Details of modelling this viscous force are presented in the following section.

Modelling of the viscous force

In the equation of motion, viscous effects are modeled as an additional quadratic damping source. It is written:

$$F_{viscous}=-\frac{1}{2}C_D A\left(\dot{X}-\dot{X}_0\right)^2 \tag{2}$$

With:

- A being the area perpendicular to the motion, in our case it is h.ℓ
- C_D the drag coefficient
- $\dot{X}_0$ the velocity of the incident wave field.

Estimation of the viscous damping coefficient

The drag coefficient depends on the geometry and on the conditions of the flow. Therefore a non-dimensional Keulegan Carpenter number (KC) becomes relevant. The KC number is defined as;

$$KC=U_m T/D \tag{3}$$

Where U_m is amplitude of the velocity of moving structure, T the time period and D the relevant dimension of the rigid structure. For an oscillating flow, KC number can be written as (Sumer and Fredsoe, 2006).

$$KC=2\pi a/D \tag{4}$$

When considering the above mentioned viscous force (Eq. 2) the drag coefficient is a prerequisite which can be chosen from literary resources or, alternatively, one could adopt the experimental procedure. However CFD does provide an alternative to the complex and time consuming experimental setup. In this work Flow3d – a commercial CFD package – has been used for the viscous force calculations and the CFD lead values of the force coefficient have been consulted along with the published experimental and numerical work. A validation study of the CFD model for an oscillatory heaving cylinder has already been presented (Bhinder et al, 2011).

The CFD solver is based on RANSE (Reynolds Averaged Navier Stokes Equations) and therefore the viscous force is automatically being treated in the equation of motion. Flow3d has previously been used for wave propagation applications including floating wave energy converter (Bhinder et al, 2009). Further details on the solver and the meshing methodology can be traced in (Flow3d Manual, 2011). The methodology of the drag constant estimation comprised the best fit of the two forces, the Morison force and the CFD viscous force, in addition the least square best fit method have been employed for the curve fitting analysis. For a 3d oscillating structure in stationary fluid the Morison equation – a semi-empirical formulation – is written as (Uzunoglu et al, 2001)

$$F(t)=-\frac{1}{2}\rho AC_D\dot{x}|\dot{x}|-\rho VC_I\ddot{x} \tag{5}$$

Were A is the area and V is the volume of the moving object. Here C_D and C_I are drag and inertia coefficients respectively. For a fixed body in oscillating fluid the inertia coefficient becomes $C_m=1+C_I$.

Calculation of the APP

Once one has been able to estimate the *Cd*, the equation of motion (Eq. 1) can be solved. In this study, it was done using the MATLAB solver ode45. Subsequently, the instantaneous power ($P_{inst}(t)$) is given by

$$P_{inst}(t)=B_{pto}\dot{X}(t)^2 \tag{6}$$

Over the duration of the simulation, the mean power ($\overline{P}_T(H_s,T_p)$) is as follows:

$$\overline{P}_T(H_s,T_p)=\frac{1}{T}\int_0^T p_{inst}(t)dt \tag{7}$$

Then, the Annual Power Production (APP) of the device is examined in accordance with the Yeu island site where the irregular sea states are described by the Bretschneider spectrum defined as

$$\left.\begin{aligned}S(f)&=\frac{A}{f^5}e^{\frac{-B}{f^4}}\\ A&=\frac{5}{16}\frac{H_s^2}{T_p^4}\quad ,B=\frac{5}{4}\frac{1}{T_p^4}\end{aligned}\right\} \tag{8}$$

Here *Hs* and *Tp* refer to significant wave height and peak wave period respectively. The sea state statistics $C(H_s,T_p)$ of the Yeu island site located on the west coast of France are shown by the scatter diagram of (Fig. 2). Using these statistics and Eq. 7, finally the annual power production (APP) of the device is calculated by;

$$APP = \sum_{H_s} \sum_{T_p} \bar{P}_T \left(H_s, T_p \right) C\left(H_s, T_p \right) \quad (9)$$

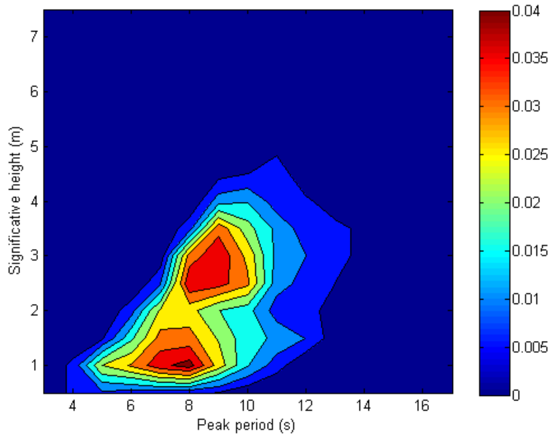

Fig. 2 Contour plot of sea state at the Yeu site

RESULTS

Estimation of the viscous damping coefficient using CFD

Case studies considered for the CFD simulations are shown in Table1.

Table 1. CFD simulations case studies

Case-Study	Amplitude	Period	KC
B1	1 m	6 s	0.6
B2	2 m	7.7 s	1.6
B3	3 m	10 s	3.0

For a typical simulation the dimensions of the computational domain were X (horizontal) = 120m, Y = 30m, and Z (vertical) =40m with number of cells being 1073600 where the smallest cell size was 0.4m. However stretched cells were placed adjacent to the boundaries of the domain so that to minimize the reflection effect (see Fig. 3). Moreover due to symmetrical representation only half of the device was modelled along the y-direction (i.e. length of the device, see: Fig.1). Specifications of the computational resource used in this study are as follows;

Ram: 6GB, processor: Intel(R) Xeon(R) CPU E5620 @2.40GHZ 2.39GHZ , System: Windows 7 Professional 64 bits.
For a 60s simulation the CPU time was recorded to be 58.16 min.

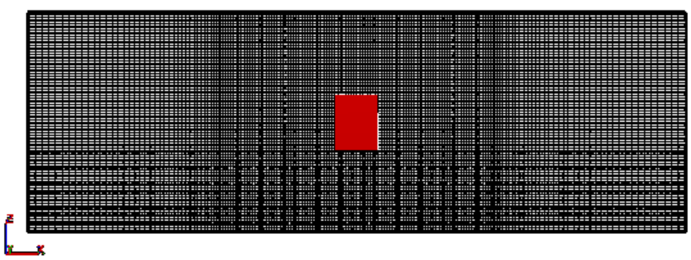

Fig. 3 Computational domain of the CFD simulations

Mesh independence of the results reported was insured by convergence check (see: Table 2). Following results of mesh convergence test Mesh1 (of Table. 2) was chosen for all simulations.

Table 2. Mesh convergence test for case B2

Mesh	Total cells	Smallest cell	*Cd*	*Cm*
1	1073600	0.4	1.85	1.81
2	2857372	0.3	1.85	1.83
3	6026000	0.2	1.87	1.83

Fig. 4 to 6 show the fluid force applied on the body calculated with Flow3D and the best fit of this force obtained using the Morison equation. The agreement of the two forces appear to be of rather good quality in the first two cases (Fig. 4 and 5) and reasonably acceptable in the last case (Fig. 6).

For each case-study the evaluated drag coefficients and added mass coefficients are shown in Table 3. One can see that the order of magnitude of the drag coefficient is found to be about 2. It is also observed that *Cd* decreases with an increasing KC number whereas the added mass coefficient is almost constant, i.e. 1.8.

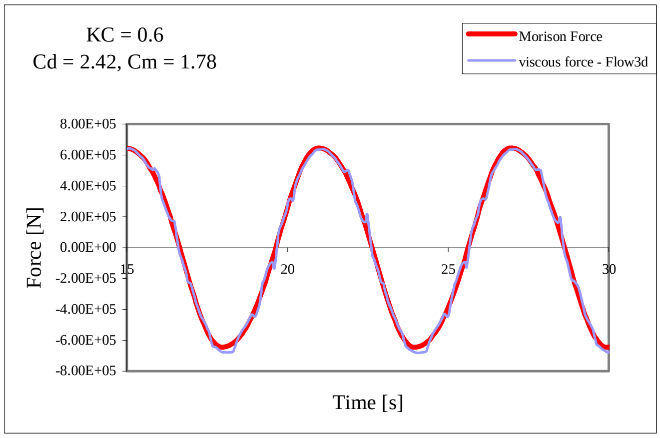

Fig. 4 Force comparison for case study B1

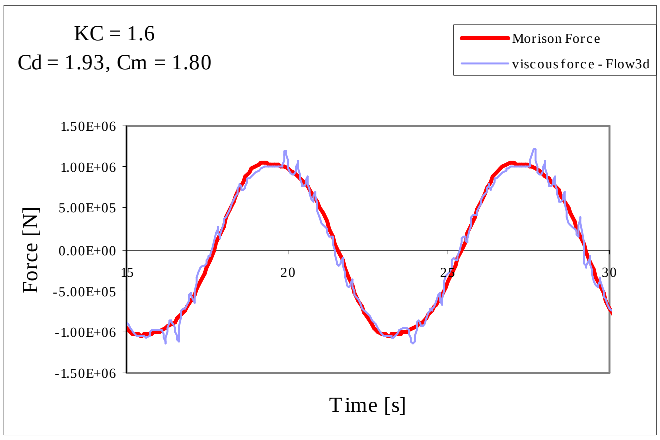

Fig. 5 Force comparison for case study B2

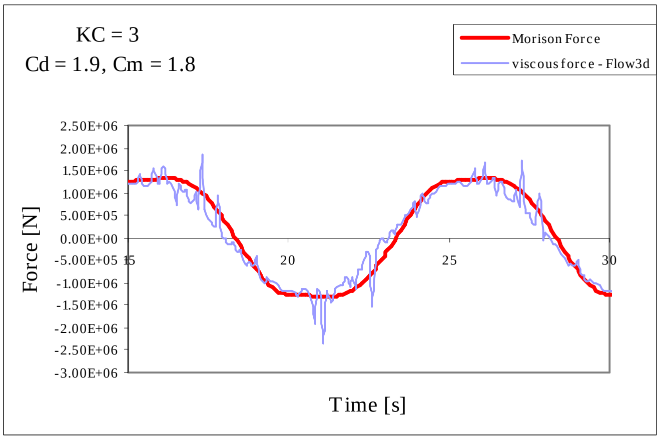

Fig. 6 Force comparison for case study B3

Table 3. Drag coefficients for the surging WEC obtained via CFD

Case-Study	*Cd*	*Cm*
B1	2.42	1.78
B2	1.93	1.8
B3	1.9	1.8

Contour profiles of dissipation of the turbulent energy in the vicinity of the oscillating device reveals the generation of a vortex formation around each sharp corners. The turbulent energy dissipation of the first 2-cycles of oscillation for case B3 is shown in Fig. 7.

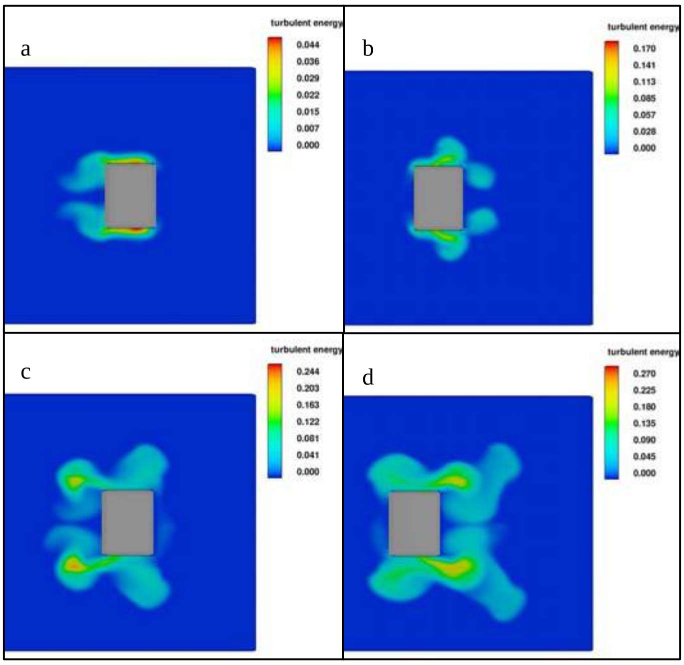

Fig. 7 Turbulent energy around surging device at various time instants for case study B3; (a) t =4.9s, (b) t =7.4s, (c) t =14.2s, (d) t =18.8s

Since the dimensions of the WEC resemble a square cylinder therefore these CFD results can be consulted by juxtaposition of our results with the one's present in Table 4 which has been taken from the work of (Zheng and Dalton, 1999) where drag and inertia forces for a square cylinder have been presented along with references from experimental work. Although the order of magnitude is similar, one can see that in our case the observed drag force is lower than results obtained by these authors.

Table 4. Drag coefficient for oscillating flow past square cylinder (Zheng and Dalton, 1999)

KC	Zheng & Dalton calculated *Cd*	Scolan & Faltinson calculated *Cd*	Bearman et al. experimental *Cd*
1	3.01	4.39	3.19
2	3.21	3.61	3.15
3	3.19	3.19	2.84

Fact that the width of the WEC is smaller than the other two equal dimensions, this differentiates our case-study from that of a square cylinder hence a higher value of the *Cd* was expected. The reason why the magnitude of this drag coefficient is lower than the case of a square cylinder is under investigation.

Effect of viscous force on the APP of the WEC

Overall picture of performance of the WEC is shown via numerically computed power matrix (Fig. 8) which gives the average value of power production for each corresponding set of *Hs* and *Tp*. It is reasonably prominent that when viscous damping is taken into account the predicted performance is reduced to almost 60 %. Also the corresponding absorbed power as a function of wave frequency is shown in Fig.9 where the lower peak of the absorbed power refers to viscous force scenario.

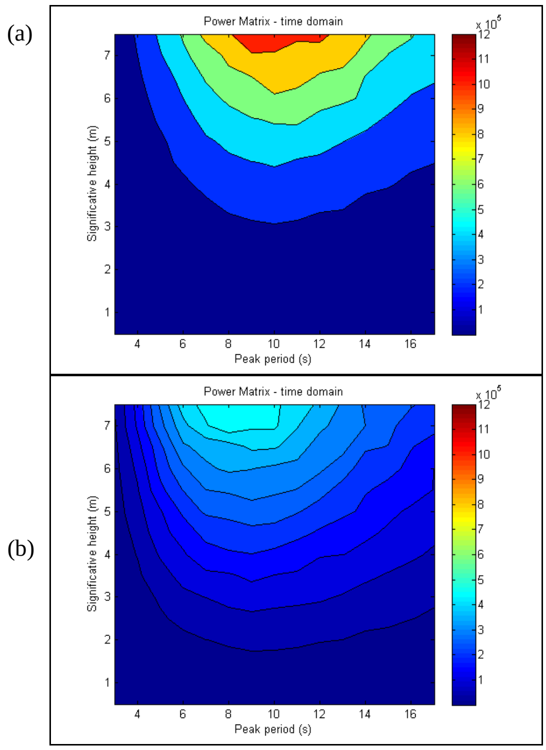

Fig. 8 Contour plots of the power matrix; (a) without drag term, Cd=0, (b) with drag term,Cd=1.8

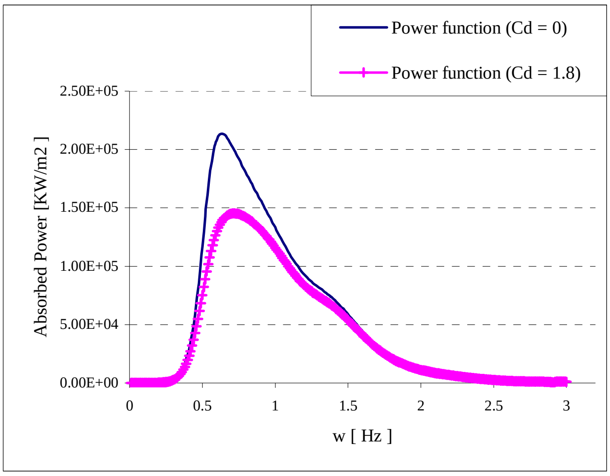

Fig. 9 Power function with and without drag damping

Finally comparison of the power production with and without viscous term has been shown in Table 5.

Table 5. Table captions

Power Output	Without viscous drag	With viscous drag *Cd*=1.8
APP	114 KW	74.4 KW

It is shown that the viscous drag (*Cd* = 1.8) causes quite significant loss (i.e. 34.7%) in the APP of this specific device. In real sea scenario the instantaneous values of exact KC number cannot be determined however for a specific device at precise location a range of possible KC values can be evaluated following sea statistics and device dimensions. Then power loss against possible values of the expected drag range would provide a better insight into the design of the WECs. For this, *Cd* was successively increased and the corresponding APP has been plotted as shown in Fig.10.

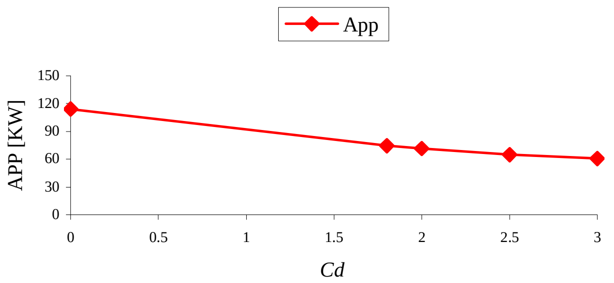

Fig. 10 APP for various *Cd* values

Note that the APP output is usually site dependent. Here input sea statistics correspond to the Yeu island site therefore at other locations the impact of the viscous drag might be different. This scenario would be analysed as part of future work.

CONCLUSIONS

Presented results show that CFD is a viable option for evaluating viscous drag coefficient of a particular wave energy converter. However one needs to make sure that for a given structure the drag coefficient does not differ much when the test case includes wave propagation as is currently being investigated.

Following the methodology presented here the drag coefficient of any complex shaped structure can be deduced using CFD and then the time-domain model offers a robust approach for numerical modelling of the WECs. Otherwise a comprehensive simulation of irregular wave propagations using CFD is somewhat challenging and time consuming.

In this study the WEC responds only in one degree of freedom and in this case PTO is also providing considerable damping but even so the power loss due to the viscous phenomenon is significant. Thus for one degree of motion WEC especially for flap type devices it has been demonstrated that the viscous drag plays an important role and hence requires further examination. However for pitching devices the role of viscous drag might be different and would be dealt with in future studies.

ACKNOWLEDGEMENTS

The authors gratefully acknowledge that this contribution is made possible under the Marie Curie Initial Training Network ‘wavetrain2 project’, financed by the FP7 of the European Commission (contract-No: MCITN-215414).

REFERENCES

Babarit, A (2010). " Impact of Long Separating Distances on the Energy Production of Two Interacting Wave Energy Converters, " *J. Ocean Engineering*, Vol 37, pp 718-729.

Bearman, PW, Graham, JMR., Obasaju, ED & Drossopoulos, GM (1984). "The Influence of Corner Radius on the Forces Experienced by Cylindrical Bluff Bodies in Oscillatory Flow, "*Applied Ocean Research*, Vol 6, pp 83-89.

Bhinder, MA, Mingham CG,Causon, DM, Rahmati, MT, Aggidis, GA, Chaplin, RV (2009). "Numerical Modelling of a Surging Point Absorber Wave Energy Converter," *Proceedings of 8th European Wave and Tidal Energy Conference,EWTEC*,Uppsala, Sweden.

Bhinder, MA, Babarit, A, Gentaz, L, Ferrant, P (2011), "Assessment of the Viscous Damping via 3D-CFD Modelling of a Floating Wave Energy Device," *EWTEC*, Southampton, UK .

Flow3D User Manual (2011), *Flow Science Inc.*Version 10.0.

Folley, M, Whittaker, T, Henry, A (2005). "The Performance of a Wave Energy Converter in Shallow Water," *6th European Wave and Tidal Energy Conference*,Glasgow,UK.

Hals, J, Taphipour, R and Moan, T (2007). "Dynamics of a Force-compensated Two-body Wave Energy converter in Heave with Hydraulic Power Take-off Subject to Phase Control," *Proceedings of the 7th European Wave and Tidal Energy Conference*, Porto, Portugal 2007.

Sumer MB & Fredsoe, J (2006). "Hydrodynamics Around Cylindrical Structures,) " (Revised Edition), *World Scientific*.

Uzunoglu B, Tan, M and Price, WG (2001). "Low-Reynolds-number Flow Around an Oscillating Circular Cylinder using a Cell Viscous Boundary Element Method, " *International Journal for Numerical Methods in Engineering*, Vol 50, pp 2317-2338.